Available online at www.sciencedirect.com
SCIENCE DIRECT®
Journal of Sound and Vibration 285 (2005) 491–500
JOURNAL OF SOUND AND VIBRATION
www.elsevier.com/locate/jsvi

Short Communication

Transient response in a finite hollow cylinder from time-delayed prescribed motion at the boundary

Michael El-Raheb*

1000 Oak Forest Lane, Pasadena, CA 91107, USA

Received 28 June 2004; received in revised form 24 September 2004; accepted 29 September 2004
Available online 25 December 2004

Abstract

Previous work (Int. J. Solids Struct. 41(18–19) (2004) 5051 on transient response of a hollow cylinder to time-dependent radial motion is extended to include motion of the excitation along the axis of the cylinder.

1. Introduction

When a projectile penetrates into human tissue, it moves material by replacing it with its own volume. When the material fails, it acts more like a fluid, lessening the amount of material being compressed. In the radial direction, material is compressed by an expanding cross-section of the projectile's smoothly curved nose. As long as the projectile's speed is much smaller than the speed of stress waves in the material, the moving projectile can be approximated by radial and axial velocities prescribed along its boundary [1]. For a projectile speed of 300 ft/s and a dilatational speed in tissue material of 5600 ft/s, this approximation is valid. However, for projectile speed in excess of 1000 ft/s, projectile motion must be considered in the analysis.

The forcing function is a radial motion prescribed over part of the inner cylindrical boundary while the remaining part is traction-free. This leads to a mixed boundary value problem whose solution is briefly outlined for completeness while details may be found in Ref. [1]. In order to

*Tel.: +1 626 7965528; fax: +1 626 5838834.
E-mail address: mertrident@earthlink.net (M. El-Raheb).

0022-460X/$ - see front matter
doi:10.1016/j.jsv.2004.09.033

convert the segment of boundary where motion is prescribed to one where traction is prescribed, response from a set of unit ring tractions with time dependent weights is superimposed. These weights are updated at each time step using the condition that the combined displacement response at the center of each ring equals the prescribed instantaneous displacement. In this way, the forcing function is converted to pure traction with time varying spatial dependence.

2. Analysis

A brief outline of the principal points of the analysis follows in order to clarify how the time-delayed forcing function along the cylinder's axis is included in the algorithm. In cylindrical coordinates, the axisymmetric elastodynamic equations are

$$\mu\nabla^2\mathbf{u} + (\lambda+\mu)\nabla(\nabla\cdot\mathbf{u}) = \rho\partial_{tt}\mathbf{u}, \tag{1}$$

$$\nabla^2 \equiv \partial_{rr} + 1/r\partial_r + \partial_{zz},$$
$$\nabla \equiv (1/r\partial_r r)e_r + (\partial_z)e_z,$$

where (r, z) are radial and axial independent variables, $\mathbf{u} = \{u, w\}^{\mathrm{T}}$ is displacement vector along these directions, (λ, μ) are Lame constants, ρ is mass density and t is time. For harmonic motions in time and simply supported boundaries at $(0, l)$ the solution is

$$\begin{aligned}\bar{u}(r,z) &= [-k_e(C_1J_1(k_er) + C_2Y_1(k_er)) + k_z(C_3J_1(k_sr) + C_4Y_1(k_sr))]\cos(k_zz),\\ \bar{w}(r,z) &= [k_z(C_1J_0(k_er) + C_2Y_0(k_er)) + k_s(C_3J_0(k_sr) + C_4Y_0(k_sr))]\sin(k_zz)\end{aligned} \tag{2}$$

with constitutive relations

$$\begin{aligned}\sigma_{rr} = \lambda\Delta + 2\mu\partial_r u,\ \ \sigma_{\theta\theta} = \lambda\Delta + 2\mu u/r,\\ \sigma_{zz} = \lambda\Delta + 2\mu\partial_z w,\ \ \tau_{rz} = \mu(\partial_z u + \partial_r w),\\ \Delta = \partial_r u + u/r + \partial_z w,\end{aligned} \tag{3}$$

$k_z = m\pi/l$. Boundary conditions at $r = r_p$ and $r = r_o$ are

$$\begin{aligned}\sigma_{rr}(r_p, z, t) = p_r(t)[H(z - z_a) - H(z - z_b)],\\ \tau_{rz}(r_p, z, t) = 0,\\ \sigma_{rr}(r_o, z, t) \equiv \tau_{rz}(r_o, z, t) = 0,\end{aligned} \tag{4}$$

where $p_r(t)$ is a time-dependent uniform radial traction acting on the inner cylindrical boundary $r = r_p$ in the interval $z_a \leqslant z \leqslant z_b$.

Divide the cylindrical surface $\{r = r_p,\ z_a \leqslant z \leqslant z_b\}$ into $n+1$ equidistant ring stations with constant increment Δz_p

$$\begin{aligned}z_1,\ z_2,\ z_3, \ldots,\ z_{n+1},\ z_l - z_{l-1} = \Delta z_p = \text{const},\\ z_l = z_a + (l-1)\Delta z_p.\end{aligned} \tag{5}$$

Assume a uniform pressure of unit intensity to act over each ring segment $z_{l-1} \to z_l$. The elastodynamic solution to the kth ring pressure segment is outlined below.

For each pressure segment, expand each dependent variable in terms of eigenfunctions that satisfy homogeneous boundary conditions. Express total displacement $\mathbf{u}_k(r,z;t)$ as a superposition of two terms:

$$\mathbf{u}_k(r,z;t) = \mathbf{u}_{sk}(r,z) f_p(t) + \mathbf{u}_{dk}(r,z;t), \tag{6}$$

where $\mathbf{u}_{sk}(r,z)$ is static displacement vector satisfying (1) when time derivative vanishes, $\mathbf{u}_{dk}(r,z;t)$ is dynamic displacement vector satisfying the dynamic equation of motion (1), and $f_p(t)$ is time dependence of the forcing pressure. For each axial wavenumber m, express $\mathbf{u}_{dk}(r,z;t)$ in the eigenfunctions $\mathbf{\Phi}_{mj}(r,z)$,

$$\mathbf{u}_{dk}(r,z;t) = \sum_j \sum_m a_{mjk}(t) \mathbf{\Phi}_{mj}(r,z), \tag{7}$$

where $a_{mjk}(t)$ is a generalized coordinate of the jth eigenfunction with m axial half-waves from the kth pressure segment. Substituting (6) and (7) in (1) and enforcing orthogonality of $\mathbf{\Phi}_{mj}(r,z)$ yields uncoupled equations in $a_{mjk}(t)$. Evaluating radial and axial displacements $u_k(r,z;t)$ and $w_k(r,z;t)$ from the kth pressure segment at each central point $z_{cl} = (z_l + z_{l-1})/2$ of a pressure segment yields coefficients of the influence matrices

$$U_{lk}(t) = \sum_j \sum_m a_{mjk}(t) \bar{u}_{mjk}(r_p, z_{cl}) + u_{sk}(r_p, z_{cl}) f_p(t), \tag{8}$$

where $\bar{u}_{mjk}(r_p, z_{cl})$ and $u_{sk}(r_p, z_{cl})$ are modal and static displacement dyads at z_{cl} from the kth pressure segment. Since $f_p(t)$ is arbitrary, it was found from numerical experiments that a simple ramp is appropriate

$$f_p(t) = (t/\Delta t_1)[H(t) - H(t - \Delta t_1)] + H(t - \Delta t_1), \tag{9}$$

where Δt_1 is rise time of the first line segment in the prescribed acceleration profile shown in Fig. 2(c). Enforcing the condition of prescribed displacement $u_p(t)$ at each time step yields a set of simultaneous equations in the weights $p_k(t)$

$$\sum_{k=1}^{n} U_{lk}(t) p_k(t) = u_p(t), \quad l = 1, n. \tag{10}$$

In the case of time-delayed prescribed displacement where the projectile moves axially varying length of the footprint instantaneously, f_p depends not only on time t but also on axial coordinate z in the form

$$f_p(\hat{t}), \ \hat{t} = (t - z/V_p) H(t - z/V_p), \tag{11}$$

where V_p is projectile speed and $H(t - z/V_p)$ is the Heaviside function. The significance of (11) is that at some station z, f_p acts only when $t \geqslant z/V_p$ otherwise it vanishes thus the term "time-delayed".

Table 1
Cylinder properties

E (lb/in^2)	4.5×10^4
ρ (lbs^2/in^4)	8.7×10^{-5}
υ	0.48
l (in)	4
r_p (in)	0.25
r_o (in)	3
c_d (in/s)	6.74×10^4
c_s (in/s)	1.322×10^4

3. Results

In all results to follow, geometric and material properties of the cylinder are listed in Table 1. The footprint extends from $z_a = 0.1''$ to $z_b = 1.6''$. The properties in Table 1 yield extensional and shear wave speeds c_d and c_s 5610 and 1115 ft/s and the ratio $c_d/c_s \simeq 5$.

Fig. 1 plots prescribed radial motions at the cylinder's inner boundary from a cylindrical projectile with a spherical nose $0.25''$ in radius and $V_p = 1000$ ft/s. For a moving projectile, prescribed motion starts at one end of the cylinder and moves inward into the cylinder with the speed of the projectile as shown in Fig. 2 for three different projectile axial positions $z = 0,\ 5\Delta z_p,\ 10\Delta z_p$.

Since the plane-strain cylinder is the simplest example, it is presented first for comparison with the finite length cases. Fig. 3(a–e) plots histories of the plane-strain cylinder for the prescribed motion in Fig. 2 at three radial stations $r = r_p,\ 2r_p,\ 4r_p$. At $r = r_p$ (Fig. 3(a)), u follows the prescribed displacement in Fig. 2(a), and $\mathrm{d}u/\mathrm{d}t$ (Fig. 3(b)) follows prescribed velocity in Fig. 2(b). The first reflection from the outer boundary $r = r_o$ happens at $t \approx 80\,\mu$s as evidenced by the sudden rise in histories there. At $r = 2r_p$ and $4r_p$, u histories exhibit the time-delay in wave front from propagation with finite speed c_e. Soon after motion starts, the closeness in magnitude of peak σ_{rr}, $\sigma_{\theta\theta}$ and σ_{zz} (Fig. 3(c–e)) implies a hydrodynamic state of stress. Note the sharp rise in stress history at $t \approx 80\,\mu$s when the first reflection from $r = r_o$ is felt at the corresponding z.

Fig. 4 plots histories from prescribed motion uniform over the footprint at three different axial stations; $z = 0.25''$, $0.8''$ and $1.7''$. The first two stations lie within the length of the footprint $l_p = 1.5''$ while the $z = 1.7''$ station is outside this interval. In Fig. 4, histories of all dependent variables at each $z-$station lie along a column, while histories of a dependent variable for the three $z-$stations lie along a row. Soon after start of motion, the u histories at $z = 0.25''$ and $0.8''$ in Fig. 4(a1,a2) follow the plane-strain case in Fig. 3(a). However, the first reflection is not accompanied by sharp rises in response as in plane-strain. At $z = 1.7''$, u and $\mathrm{d}u/\mathrm{d}t$ response is attenuated as expected since that station is remote from the footprint. Magnitude of the w histories is comparable to those of u at $z = 0.25''$. However, w attenuates substantially at the other stations. An explanation is that w motion is controlled by shear waves, which for the present material are 5 times weaker than extensional waves controlling u. Soon after start of motion and within the footprint, normal stress histories (Fig. 4(d1–d3,e1–e3,f1–f3)) resemble those of the plane-strain case in that magnitude of the three stress components is approximately the same implying a hydrostatic state of stress. Agreement of results from the

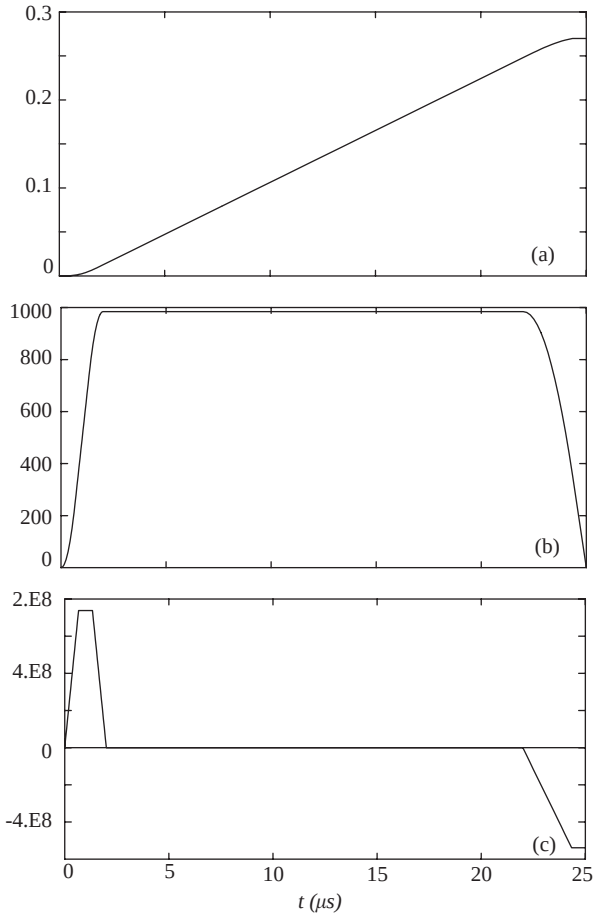

Fig. 1. Prescribed motion: (a) u_p (in), (b) $\mathrm{d}u_p/\mathrm{d}t$ (ft/s), (c) $\mathrm{d}^2u_p/\mathrm{d}t^2$ (ft/s^2).

plane-strain and finite cylinder with prescribed uniform motion implies that the plane-strain approximation is satisfactory for axial stations within the footprint. Also, magnitude of stress remote from the footprint is comparable to that within the footprint after the initial hydrostatic transient elapses.

Fig. 5 plots histories from time-delayed prescribed motion. The same nomenclature applies as in Fig. 4. Comparing histories of u and $\mathrm{d}u/\mathrm{d}t$ in Fig. 4(a1–a3,b1–b3) and Fig. 5(a1–a3,b1–b3) it is apparent that except for the shifted response at the footprint, magnitude and shape of response are the same. However, magnitude of w histories in Fig. 5(c1–c3) are almost 1/2 those in Fig. 4(c1–c3). This is caused by the reduction in shear in the time-delayed prescribed displacement compared to the uniform case. Comparing stress histories in Fig. 5(d1–d3,e1–e3,f1–f3) and Fig. 4(d1–d3,e1–e3,f1–f3) reveals that soon after start of motion, the time-delayed case looses the initial hydrostatic transient while magnitudes following this transient are comparable. This steep drop in stress across the edges of the footprint is caused by the low shear rigidity of the material consistent with the ratio $c_s/c_d \simeq 1/5$.

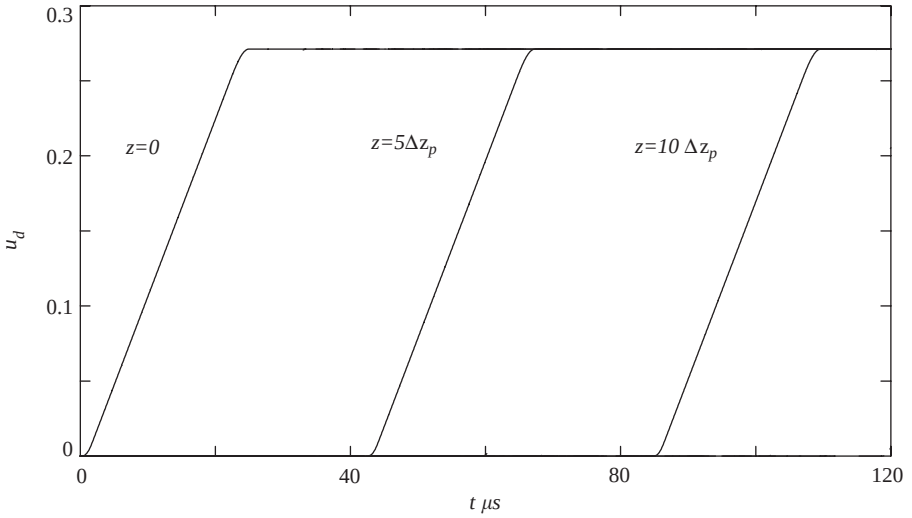

Fig. 2. Delayed prescribed displacement left line $z = 0$, middle line $z = 5\Delta z_p$, right line $z = 10\Delta z_p$.

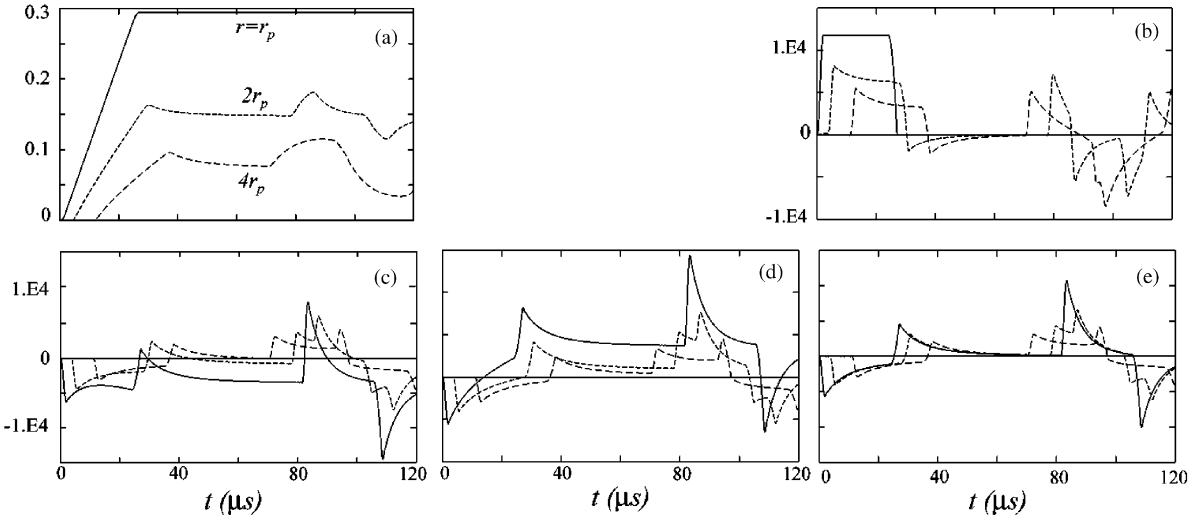

Fig. 3. Histories of plane-strain cylinder with prescribed displacement: (a) u, (b) $\mathrm{d}u/\mathrm{d}t$, (c) σ_{rr}, (d) $\sigma_{\theta\theta}$, (e) σ_{zz}.

Fig. 6 plots snap-shots of the deformed cylinder generator for the two types of excitation at 3 times $t = 40$, 80 and 110 μs. Note the expanding footprint in the case of the time-delayed case (Fig. 6(a2–c2)). Fig. 7 plots instantaneous $\sigma_{rr}(r_p, z; t_o)$ distributions for $10\,\mu s \leqslant t_o \leqslant 110\,\mu s$ in intervals of 10 μs. In both types of excitation, pressure at the ends of the footprint is higher than that at intermediate stations. For the time delayed excitation, Fig. 7(b) shows the expansion of the footprint with time following prescribed displacement in Fig. 2. The undulation in the $\sigma_{rr}(r_p, z; t_o)$

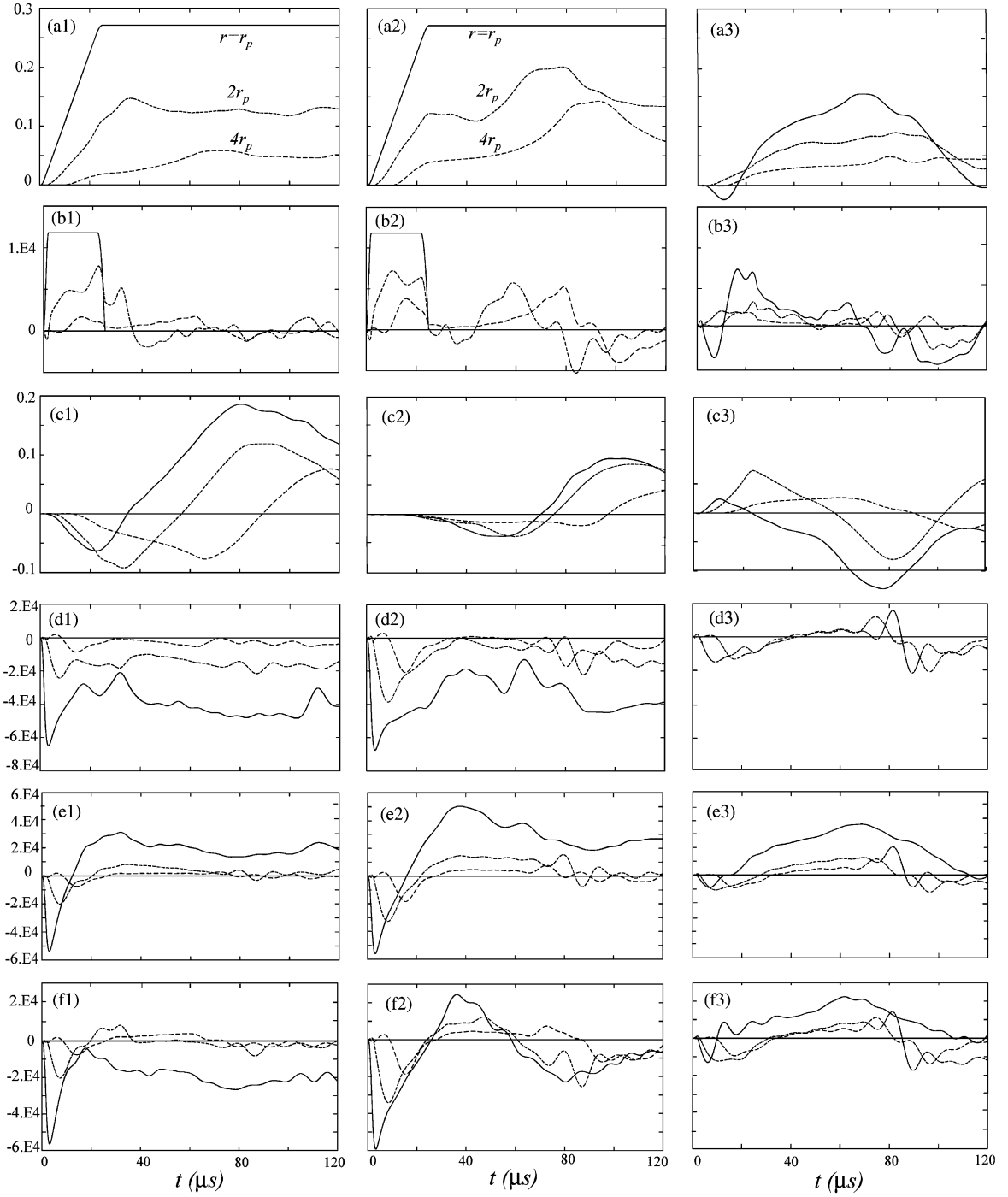

Fig. 4. Histories of cylinder with uniform prescribed displacement: (a1) u, (b1) w, (c1) $\mathrm{d}u/\mathrm{d}t$, (d1) σ_{rr}, (e1) $\sigma_{\theta\theta}$, (f1) σ_{zz} : $z = 0.25''$, (a2) u, (b2) w, (c2) $\mathrm{d}u/\mathrm{d}t$, (d2) σ_{rr}, (e2) $\sigma_{\theta\theta}$, (f2) σ_{zz} : $z = 0.8''$, (a3) u, (b3) w, (c3) $\mathrm{d}u/\mathrm{d}t$, (d3) σ_{rr}, (e3) $\sigma_{\theta\theta}$, (f3) σ_{zz} : $z = 1.7''$.

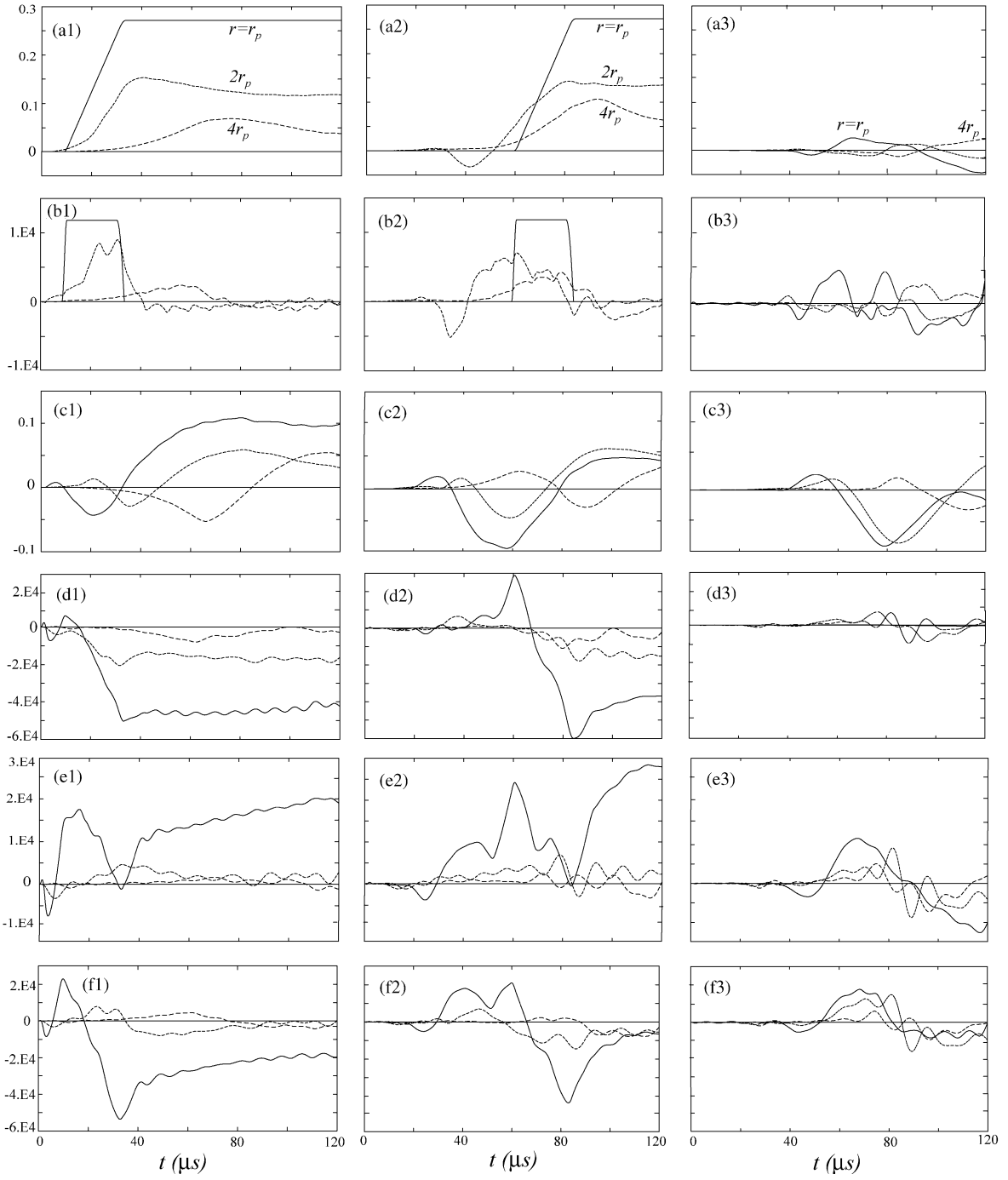

Fig. 5. Histories of cylinder with delayed prescribed displacement: (a1) u, (b1) w, (c1) $\mathrm{d}u/\mathrm{d}t$, (d1) σ_{rr}, (e1) $\sigma_{\theta\theta}$, (f1) σ_{zz}: $z = 0.25''$, (a2) u, (b2) w, (c2) $\mathrm{d}u/\mathrm{d}t$, (d2) σ_{rr}, (e2) $\sigma_{\theta\theta}$, (f2) σ_{zz}: $z = 0.8''$, (a3) u, (b3) w, (c3) $\mathrm{d}u/\mathrm{d}t$, (d3) σ_{rr}, (e3) $\sigma_{\theta\theta}$, (f3) σ_{zz}: $z = 1.7''$.

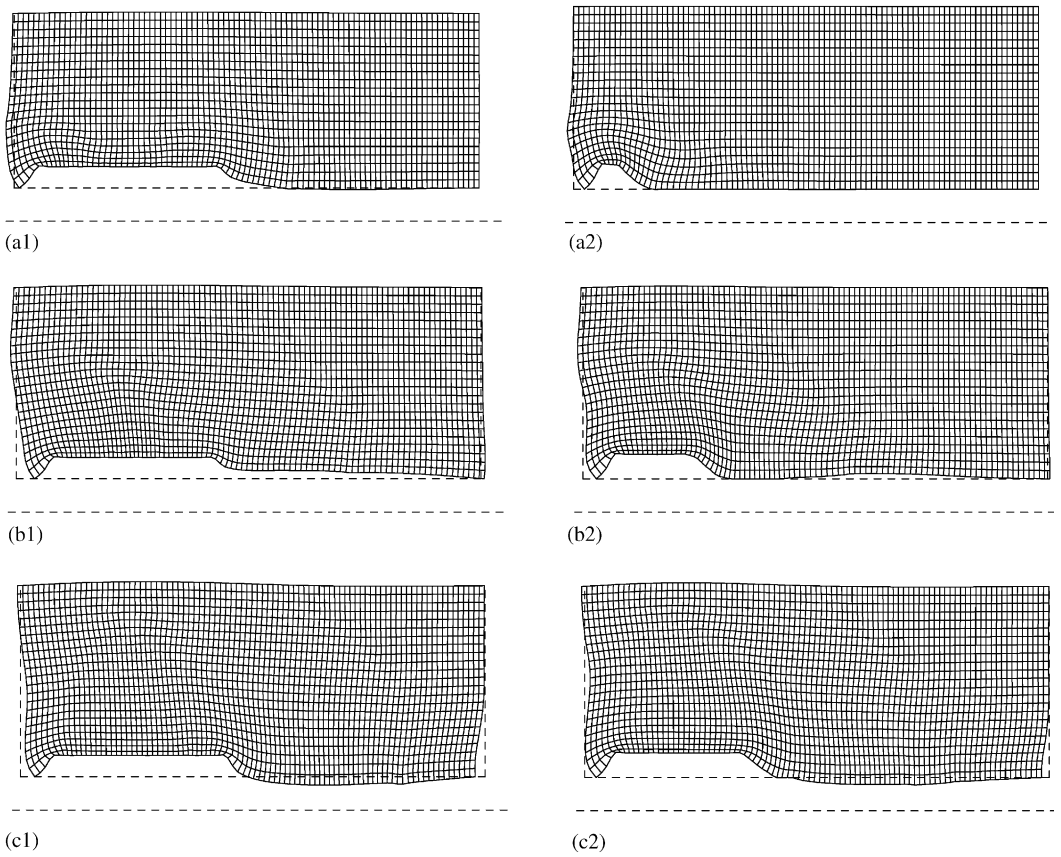

Fig. 6. Time snap-shots of cylinder with prescribed displacement: (a1) $t = 40\,\mu s$, (b1) $t = 80\,\mu s$, (c1) $t = 110\,\mu s$: uniform, (a2) $t = 40\,\mu s$, (b2) $t = 80\,\mu s$, (c2) $t = 110\,\mu s$: time-delayed.

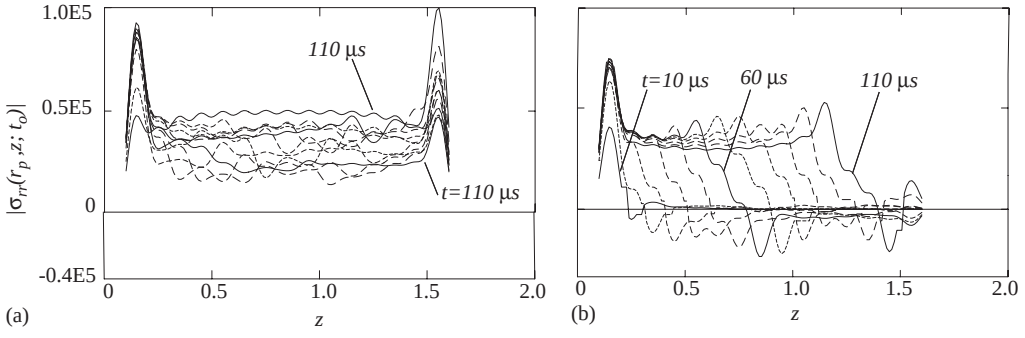

Fig. 7. Snap-shots of $|\sigma_{rr}(r_p, z; t_o)|$ distribution in cylinder with prescribed displacement at $10\,\mu s < t_o < 110\,\mu s$: (a) uniform: —— top $t = 10\,\mu s$, bottom $t = 110\,\mu s$ – – (b) time-delayed: —— far left $t = 10\,\mu s$, far right $t = 110\,\mu s$.

distribution is an artifact of the finite number of pressure ring segments dividing the footprint. The distribution becomes smoother as number of ring segments increases.

4. Conclusion

An extension to wave propagation in a hollow cylinder is presented for motion of the excitation along the cylinder's axis. Two types of excitation are considered, a uniform prescribed motion and a time delayed prescribed motion. Noteworthy results are:

(1) Soon after motion starts, the normal stress state for the plane-strain cylinder and finite cylinder with uniform prescribed displacement is almost hydrostatic. Displacement, velocity and stress responses over the footprint for these two cases are comparable.
(2) Response from time-delayed excitation is similar to that from uniform excitation in magnitude and form although the former response does not exhibit the hydrostatic state soon after motion starts.

Acknowledgments

This work was supported by a grant from DARPA, executed by the U.S. Army Medical Research and Materiel Command/TATRC Contract #W81XWH-04-C-0084.

References

[1] M. El-Raheb, Wave propagation in a hollow cylinder due to prescribed velocity at the boundary, *International Journal of Solids and Structures* 41(18–19) (2004) 5051–5069.